ISSN 0965-5441, Petroleum Chemistry, 2018, Vol. 58, No. 5, pp. 434–443. © Pleiades Publishing, Ltd., 2018.
Original Russian Text © A.P. Savost'yanov, R.E. Yakovenko, A.N. Saliev, G.B. Narochnyi, S.A. Mitchenko, I.N. Zubkov, V.N. Soromotin, V.A. Kirsanov, 2018, published in Neftekhimiya, 2018, Vol. 58, No. 3.

Supported Bifunctional Cobalt Catalysts for CO and H_2 Conversion to Fuel Fractions of Hydrocarbons

A. P. Savost'yanov[a], R. E. Yakovenko[a, *], A. N. Saliev[a], G. B. Narochnyi[a], S. A. Mitchenko[a, b], I. N. Zubkov[a], V. N. Soromotin[a], and V. A. Kirsanov[a]

[a] *Platov South-Russian State Polytechnic University, Novocherkassk, Rostov oblast, Russia*
[b] *Litvinenko Institute of Physical Organic Chemistry and Coal Chemistry, Donetsk, Ukraine*
**e-mail: jakovenko@lenta.ru*

Received August 25, 2017

Abstract—of Supported bifunctional cobalt catalysts for the direct conversion of synthesis gas to liquid fuel-fraction hydrocarbons (HCs) have been studied. The effect of ZSM-5 zeolite in the structure of the support preformed using a boehmite binder on the catalytic and physicochemical properties of the catalysts has been examined. The synthesized catalysts exhibit high mechanical strength; therefore, they can be used in tubular Fischer–Tropsch (FT) synthesis reactors. The efficiency of the supported bifunctional Co/(Al_2O_3–ZSM-5) catalysts is determined by the number of active metal cobalt sites, the degree of dispersion of the cobalt crystallites, and the total surface acidity. An increase in the catalyst acidity leads to an increase in the fuel fraction selectivity owing to long-chain HCs. At the same time, the activity of the catalysts decreases; therefore, a decrease in their efficiency is observed. It is assumed that this finding is attributed to the diffusion limitations between the HC synthesis and hydrotreating sites.

Keywords: Fischer–Tropsch synthesis, bifunctional cobalt catalysts, zeolite, cracking, isomerization, synthetic hydrocarbons, motor fuels

DOI: 10.1134/S0965544118030143

Keen demand for liquid motor fuels is attributed to the global increase in the consumption of this product and the depletion of reserves of oil, which is the main feedstock for the production of this fuel [1]. In this context, alternative carbon-containing sources for the production of high-quality motor fuels (biomass; coalmine methane; natural, associated petroleum, and shale gases; and coal) are attracting ever-increasing interest of researchers [2–5]. Advantages of these types of carbon-containing feedstocks are their significant reserves, relative cheapness, and—in the case of biomass—renewability. In the foreseeable future, motor fuel technologies using these resources can become competitive with the production of these fuels from natural oil.

The well-known technology of production of synthetic hydrocarbons (HCs) by the Fischer–Tropsch (FT) method [6] is the most attractive for producing motor fuels using the above feedstock sources. The process includes several stages: the production of synthesis gas, the synthesis of HCs by the FT method, and the hydrotreating of the synthesis products (cracking of macromolecular HCs, isomerization) [7]. In general, the efficiency of the technology is determined by the intensity of the processes that occur at each of the stages and their technological and instrumental design.

One of the main tasks in the development of a technology for the production of synthetic fuels is the control of selectivity for products at the HC synthesis stage. In the presence of "classical" commercial FT catalysts based on cobalt and iron, the molecular weight distribution of the synthesized products is typically described by the Anderson–Schulz–Flory (ASF) equation [8], according to which the selectivity for gasoline (C_5–C_{11}) and diesel (C_{10}–C_{18}) fractions is limited to values of 45 and 30%, respectively. To increase the efficiency of the condensed HC production stage, synthesis is conducted under conditions providing a high probability of the HC chain propagation of $\alpha > 0.9$, which characterizes the HC distribution in the ASF equation. In this case, a significant amount of macromolecular paraffins (C_{18+}) is produced and an additional step of HC hydrotreating is required to increase the yield of liquid HCs.

A strategy in the development of a less energy-intensive and more efficient technology is to adjust the process selectivity to the desired products by selecting catalyst systems and conditions providing a single-step production of fuel fractions. In the case of direct synthesis of fuel fractions from synthesis gas over bifunc-

tional catalysts, a separate stage of hydrotreating is not required because these catalysts combine the functions of synthesis and hydrotreating of HCs [9–12]. The use of cheap feedstocks, in combination with the reduction of technological stages, makes it reasonable to expect competitive advantages of XTL technologies (conversion of any carbon-containing feedstock to liquid HCs) in the production of liquid HCs from a feedstock that is alternative to crude oil.

Extensive studies aimed at designing and optimizing bifunctional catalysts are being conducted [13–16]; a number of reviews have been published [17, 18]. A key parameter that determines the efficiency of these catalyst systems is the degree of contact of the HC synthesis sites (FT component) with the isomerization and cracking sites (acid component). The authors of [19] believe that the maximum process intensity in the presence of bifunctional catalysts is achieved if the chemical conversion rate is not limited to the rate of transfer of products between these active sites. The quantitative ratio of the sites and their activity can be controlled by introducing components with pronounced acid properties, such as HZSM-5, HY, and Hβ zeolites, which are used in commercial HC isomerization and cracking processes, into the catalyst [20].

With respect to the type of contact between the active sites, catalysts can be classified as mixed, core–shell, and impregnated [18]. The tightest contact between the active sites is provided by impregnated catalysts owing to the direct dispersion of the active component onto the zeolite. Bifunctional impregnated cobalt catalysts, in which the active component is deposited directly on an acid support, have been the focus of many studies (see [21–27]). However, it should be noted that, in most of the studies, zeolites are used in the form of a powder without any binder; these catalyst systems exhibit low mechanical properties (strength, abrasion, etc.); therefore, they are of little use for practical applications.

The aim of this study is to determine the effect of addition of the ZSM-5 zeolite into the structure of a support preformed using a boehmite binder on the catalytic and physicochemical properties of a bifunctional impregnated cobalt catalyst for the single-stage FT synthesis of motor fuel fractions of HCs.

EXPERIMENTAL

Catalyst Synthesis Procedure

Catalyst samples were synthesized on preformed supports. The supports were prepared by mixing powders of the ZSM-5 zeolite in the proton form (Ishimbay Specialized Chemical Catalyst Plant, SiO_2/Al_2O_3 = 40) and boehmite Al(OH)O (Sasol, TH 80). To provide plasticization, a water–alcohol solution of triethylene glycol with nitric acid (0.1 mol/mol Al_2O_3) was added to the mixture; the resulting mass was stirred to obtain a paste. The paste was extruded to form cylindrical pellets of the support with a diameter of 2 mm and a length of 3 mm; the pellets were air-dried at a temperature of 25°C for 24 h and subjected to a heat treatment in the following mode: at 80°C for 4 h and then at 100, 120, and 140°C for 1 h at each of the temperatures; after that, the pellets were calcined at 500°C in an air atmosphere for 4 h to provide the transition of boehmite to Al_2O_3.

The supports were impregnated with an aqueous solution of cobalt nitrate with a concentration of 55% at a temperature of 70°C for 0.5 h. The catalysts were dried at 80°C for 4 h and then at 100, 120, and 140°C for 1 h at each of the temperatures; after that, the catalysts were calcined at 400°C for 4 h.

Catalyst Testing Procedures

HCs were synthesized in a flow isothermal reactor with a fixed-bed catalyst (10 cm^3) diluted with 30 cm^3 of quartz crumb at a pressure of 2.0 MPa. Before the catalytic tests, the test samples were reduced in a hydrogen flow at a temperature of 400°C and a gas hourly space velocity (GHSV) of 3000 h^{-1} for 1 h. After that, the catalysts were activated with synthesis gas at a ratio of $H_2/CO = 2$ at a pressure of 2.0 MPa and a GHSV of 1000 h^{-1} with a stepwise rise in temperature from 180 to 240°C (2.5 °C/h). After catalyst activation, the synthesis products were poured off from the collectors and subjected to comparative balance tests at a constant temperature (240°C), GHSP = 1000 h^{-1}, P = 2.0 MPa, and a continuous on-stream time of 100 h.

Analysis of the composition of the gaseous synthesis products was conducted by gas adsorption chromatography on a Kristall 5000 chromatograph (Chromatec, Russia) equipped with a thermal conductivity detector and two columns; one of the columns (Haysep R) was used for determining C_1–C_5 HCs and CO_2 (carrier gas, helium; flow rate, 15 mL/min); the other column (molecular sieves NaX) was intended for the determination of CO, H_2, and N_2 (carrier gas, argon; flow rate, 15 mL/min). Temperature programming at a heating rate of 8°C/min was used.

The condensed synthesis products were distilled at atmospheric pressure to separate three fractions, namely, IBP of 180°C, 180–330°C, and bottoms (>330°C). The composition of the derived C_{5+} HC fractions was determined by capillary gas–liquid chromatography–mass spectrometry using an Agilent GC 7890 gas chromatograph equipped with an MSD 5975C mass-selective detector and an HP-5MS capillary column.

Cobalt content in the catalyst samples was determined by X-ray fluorescence analysis (XFA) on a Thermo Scientific ARLQUANT'X spectrometer in an

Table 1. Composition and physicochemical characteristics of the catalysts

No.	Sample	Catalyst composition, wt %			S_{sp}, m^2/g	Compression strength, MPa	
		Co*	Al_2O_3**	ZSM-5**		edge compression	compression along generatrix
1	Co/Al_2O_3	17.5	76.2	0	128.2	4.2	2.2
2	$Co/(Al_2O_3–10ZSM-5)$	17.9	68.0	7.6	130.3	6.2	–
3	$Co/(Al_2O_3–30ZSM-5)$	17.3	53.5	22.9	182.0	8.1	4.3
4	$Co/(Al_2O_3–60ZSM-5)$	18.9	29.7	44.6	245.5	7.4	5.0

* According to XFA.

** Calculated data.

air medium using a Teflon substrate with an effective irradiation area of 48.9 mm^2.

The phase composition of the catalyst samples was determined by X-ray powder diffraction (XRD) analysis on a Thermo Scientific ARL X'TRA powder diffractometer using monochromatized CuK_α radiation in the 2θ range of 5°–80° using PDF-2 [28] in the Crystallographica software system.

The morphology and microelement composition of the catalyst surface was studied by scanning electron microscopy (SEM) on a Quanta 200 SEM instrument (FEI, United States) equipped with an EDAX Genesis energy-dispersive analysis system at an accelerating voltage of 30 kV.

Transmission electron microscopy (TEM) studies of the catalysts were conducted on a Tecnai G^2 Spirit BioTWIN microscope (FEI, United States) at an accelerating voltage of 120 kV. The samples were preliminarily reduced with a nitrogen–hydrogen mixture (5 vol % H_2) under linear heating from room temperature to 500°C for 1 h. The degree of reduction of the catalysts was determined by pulsed oxidation of the reduced catalysts with a gas mixture composed of 30% O_2 and 70% He.

The textural characteristics of the catalyst surfaces were determined on a Micromeritics ChemiSorb 2750 instrument. The sample was preliminarily degassed in a helium stream at 200°C for 1 h to remove moisture and other adsorbed gases. Specific surface area was determined by the BET method using argon as an adsorbate (at a temperature of –196°C).

Analysis of the catalysts by temperature-programmed reduction (TPR) was conducted on a Micromeritics ChemiSorb 2750 instrument. The catalyst samples were degassed in a helium atmosphere at a temperature of 200°C for 1 h. Reduction was run in a stream of a gas mixture composed of 5% H_2 and 95% N_2 (20 mL/min) under linear heating from room temperature to 800°C at a rate of 20°C/min.

Ammonia adsorption was run at room temperature in a stream of an ammonia–helium mixture (20 vol % NH_3) at room temperature for 1 h. Before adsorption, the catalyst samples were degassed in a helium stream at 200°C for 1 h. Physically adsorbed ammonia was removed in a helium stream at 100°C for 0.5 h. Ammonia desorption was run in a temperature range of 100–700°C under linear heating at a rate of 20°C/min using helium as a carrier gas.

Compression tests were conducted using an IPG-1 extensometer. The average strength of the pellets (in MPa) was calculated for 20 separate measurement results.

RESULTS AND DISCUSSION

For the studies, supported catalyst samples with a ZSM-5 zeolite content in the support of 0, 10, 30, and 60 wt % were prepared. Characteristics of the bifunctional catalyst samples are shown in Table 1.

The cobalt loading in the catalyst samples varies in a range of 17.3–18.9 wt %. With an increase in the zeolite content in the support, the textural characteristics of the samples change as follows: the specific surface area increases from 128.2 to 245.5 m^2/g and the mechanical strength slightly increases with respect to the sample containing no zeolite.

The catalytic properties of the supported catalysts were studied at a continuous on-stream time of no less than 100 h (Table 2).

The highest activity in the synthesis was exhibited by the Co/Al_2O_3 catalyst sample containing no zeolite. In the presence of this sample, the CO conversion was 57.2%, while the selectivity and efficiency with respect to C_{5+} HCs were 73.1% and 79.4 kg/(m^3_{cat} h), respectively. The introduction of the zeolite into the Co/Al_2O_3 catalyst composition leads to a decrease in the catalyst activity: the CO conversion decreases to 34.2%, while the selectivity for gaseous C_1–C_4 products increases owing to a contribution of secondary reactions, in particular, the HC (hydro)cracking; ultimately, these processes lead to a decrease in the efficiency with respect to C_{5+} HCs to 49.1 kg/(m^3_{cat} h).

Table 2. Catalytic properties of the catalyst samples as a function of the ZSM-5 zeolite content in the support at GHSV = 1000 h^{-1}, $T = 240°C$, and $P = 2.0$ MPa

No.	Samples	CO conversion, %	Selectivity, %				Efficiency with respect to C_{5+}, $kg/(m^3_{cat}\ h)$
			CH_4	C_2–C_4	CO_2	C_{5+}	
1	Co/Al_2O_3	57.2	16.2	9.6	1.1	73.1	79.4
2	$Co/(Al_2O_3$–10ZSM-5)	46.5	23.4	10.5	2.2	63.9	64.7
3	$Co/(Al_2O_3$–30ZSM-5)	36.8	23.5	15.0	1.8	56.7	50.5
4	$Co/(Al_2O_3$–60ZSM-5)	34.2	22.8	13.1	1.6	62.5	49.1

Table 3. Fractional composition of the synthesis products in the presence of supported catalysts containing different amounts of the zeolite

No.	Samples	Fractional composition of C_{5+} HCs, wt %		
		IBP of 180°C	180–330°C	>330°C
1	Co/Al_2O_3	25.6	51.7	22.7
2	$Co/(Al_2O_3$–10ZSM-5)	34.7	43.7	21.6
3	$Co/(Al_2O_3$–30ZSM-5)	41.8	46.2	12.0
4	$Co/(Al_2O_3$–60ZSM-5)	47.8	44.6	7.6

Table 3 shows data on the fractional composition of C_{5+} HCs.

Macromolecular HCs with a boiling point of more than 330°C in an amount of 22.7% and HCs of the gasoline and diesel fractions in an amount of 25.6 and 51.7%, respectively, were found in the synthesis products in the presence of the Co/Al_2O_3 catalyst. The introduction of the zeolite into the Co/Al_2O_3 catalyst composition leads to an increase in the gasoline fraction (up to 47.8%) owing to the cracking of macromolecular HCs and, partially, HCs of the diesel fraction. The cracking ability of the catalysts increases after the addition of the zeolite; in this case, the content of HCs with a boiling point of >330°C monotonically decreases to a value that is 3 times lower than that for the catalyst containing no zeolite. The molecular weight distribution of HCs for the tested samples is shown in Fig. 1.

Liquid HCs for the Co/Al_2O_3 catalyst are mostly represented by normal alkanes (93.7%). The presence of a small fraction of isoalkanes and alkenes in the synthesis products is apparently attributed to the intrinsic acidity of alumina (Fig. 1a, Table 4). The introduction of the zeolite into the Co/Al_2O_3 catalyst composition contributes to the occurrence of isomerization reactions. Figures 1b–1d and Table 4 show that liquid HCs produced in the presence of the zeolite-containing catalysts contain a significant amount of isomers, as evidenced by the *iso*/*n* parameter. An increase in the olefin content in the products is associated with the occurrence of cracking reactions. The highest olefin-to-paraffin (o/p) ratio—0.446—is observed for the $Co/(Al_2O_3$–60ZSM-5) sample; it is an order of magnitude higher than the ratio in the case of the catalyst containing no zeolite.

A decrease in the isoalkane content in the composition of the synthesis products in the presence of the $Co/(Al_2O_3$–60ZSM-5) catalyst sample containing the largest amount of the zeolite can be attributed to the

Table 4. Group composition of the synthesis products

No.	Samples	Content, %			*iso*/*n*	o/p
		n-alkanes	isoalkanes	olefins		
1	Co/Al_2O_3	93.7	1.9	4.4	0.02	0.046
2	$Co/(Al_2O_3$–10ZSM-5)	84.1	12.6	3.3	0.15	0.034
3	$Co/(Al_2O_3$–30ZSM-5)	62.8	28.0	9.2	0.45	0.101
4	$Co/(Al_2O_3$–60ZSM-5)	55.3	13.8	30.8	0.25	0.446

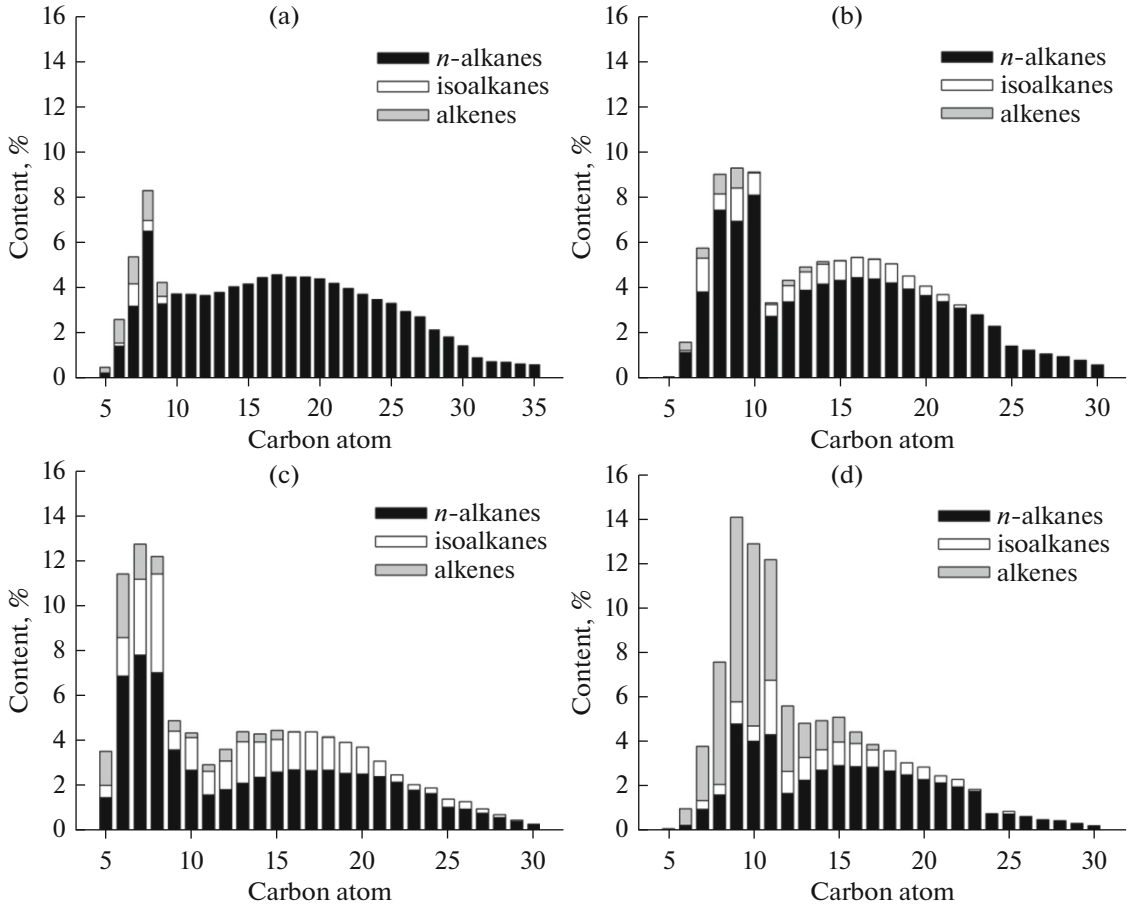

Fig. 1. Molecular weight distribution of the synthesis products in the presence of catalyst samples: (a) Co/Al_2O_3, (b) $Co/(Al_2O_3$–10ZSM-5), (c) $Co/(Al_2O_3$–30ZSM-5), and (d) $Co/(Al_2O_3$–60ZSM-5).

lower hydrogenation rate of isoolefins formed during the cracking of the primary products of FT synthesis.

The tested catalyst samples were characterized by XRD, SEM, TEM, TPR, and NH_3 TPD methods. Figure 2 shows X-ray diffraction patterns of unreduced catalysts. All of them exhibit pronounced diffraction reflections of Co_3O_4 in an angle range of $2\theta \approx 18°$–$58°$. The samples with a zeolite additive also exhibit reflections in an angle range of $2\theta \approx 7°$–$23°$ corresponding to the ZSM-5 zeolite. The Al_2O_3 phase is represented by two reflections at $2\theta \approx 55°$–$65°$. The average size of Co_3O_4 crystallites was calculated for a characteristic line with a 2θ value of 36.9° according to the Scherrer equation [29].

The Co_3O_4 crystallite sizes are in a range of 16–19 nm.

SEM microphotographs of the surface of the catalysts in the oxide form (Fig. 3) showed a significant difference in the sample surfaces. The Co/Al_2O_3 catalyst is characterized by a more uniform surface; the addition of the zeolite into the catalyst composition leads to a significant change in the surface morphology. The effect of the zeolite on morphology is most pronounced for the $Co/(Al_2O_3$–60ZSM-5) sample, which has the highest zeolite content (Fig. 3d).

The addition of the zeolite into the catalyst composition leads to a considerable change in the content of silicon and aluminum: the fraction of silicon increases to 22.9%; accordingly, the aluminum content decreases from 33.6 to 15.4% (Table 5).

Results of the TPR tests are shown in Fig. 4. All the spectra exhibit two intense reduction peaks with maxima in a temperature range of 374–384°C and 622–662°C, which are hereinafter referred to as peak 1 and peak 2 (Table 6).

Reduction peaks 1 and 2 for all the catalysts correspond to the stepwise reduction of cobalt oxide Co_3O_4 to metallic cobalt Co^0 [30, 31] according to the following equations:

$$Co_3O_4 + H_2 \rightarrow 3CoO + H_2O, \quad (1)$$

$$CoO + H_2 \rightarrow Co^0 + H_2O. \quad (2)$$

The TPR spectra for the zeolite-containing samples differ from the spectra of the Co/Al_2O_3 catalyst. The temperature maximum is shifted for reaction (1)

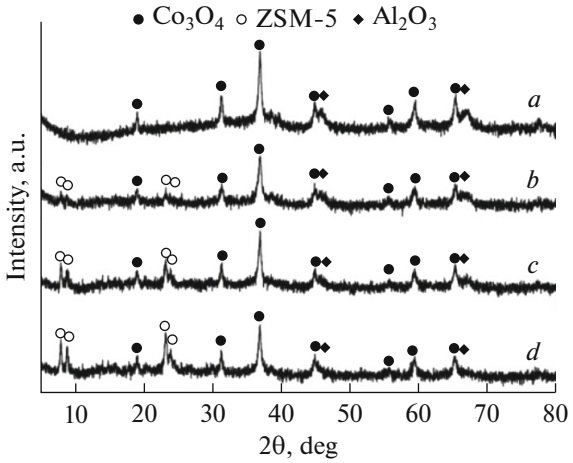

Fig. 2. X-ray diffraction patterns of the catalysts: (*a*) Co/Al_2O_3, (*b*) $Co/(Al_2O_3–10ZSM-5)$, (*c*) $Co/(Al_2O_3–30ZSM-5)$, and (*d*) $Co/(Al_2O_3–60ZSM-5)$.

(peak 1) by about 10°C toward higher temperatures. The temperature maximum of reduction for reaction (2) (peak 2) is in a temperature range of 622–662°C. The introduction of the zeolite shifts the position of peak 2 toward low temperatures owing to a decrease in the fraction of alumina in the samples: the reaction of cobalt oxide with Al_2O_3 leads to the formation of hardly reducible cobalt aluminates [32, 33]. The addition of the zeolite into the Co/Al_2O_3 catalyst leads to an increase in hydrogen absorption (Table 6); that is, the presence of the zeolite contributes to an improvement of the reducibility of the catalysts owing to the weakening of the interaction of the surface cobalt particles with the support and a decrease in the cobalt aluminate content. An increase in the area ratio (S_2/S_1) of the two base peaks from 2.05 (sample 1) to 2.54 (sample 4) suggests that the amount of hydrogen consumed for reactions 1 and 2 tends to a value of 3, which is theoretically expected on the assumption of stoichiometry of reactions (1) and (2).

For the prereduced catalysts, the size distribution of cobalt crystallites was determined by TEM (Fig. 5). The average crystallite size (nm) was calculated by the formula [34]

$$d_{av}(Co^0) = \frac{\sum n_i d_i^3}{\sum n_i d_i^2}, \quad (4)$$

where n_i is the number of particles with diameter d_i.

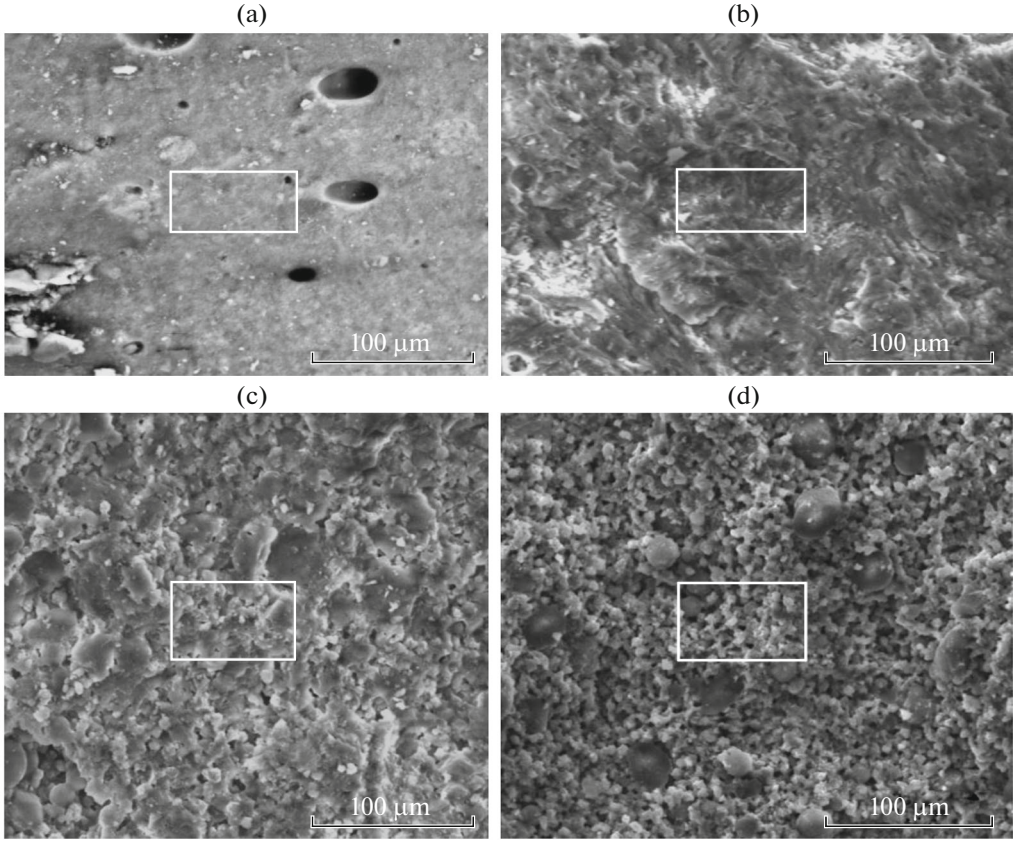

Fig. 3. SEM photographs of the surface of the catalyst samples in the oxide form: (a) Co/Al_2O_3, (b) $Co/(Al_2O_3–10ZSM-5)$, (c) $Co/(Al_2O_3–30ZSM-5)$, and (d) $Co/(Al_2O_3–60ZSM-5)$.

Table 5. Elemental composition of the selected surface area of the catalyst samples

No.	Samples	Content, wt %			
		Co	Al	O	Si
1	Co/Al_2O_3	9.4	33.6	57.0	–
2	$Co/(Al_2O_3–10ZSM-5)$	19.7	30.4	43.7	6.2
3	$Co/(Al_2O_3–30ZSM-5)$	14.9	20.2	45.0	19.9
4	$Co/(Al_2O_3–60ZSM-5)$	17.7	15.4	43.9	22.9

Table 6. TPR spectra of the catalyst samples as a function of zeolite content

No.	Catalyst	Peak 1		Peak 2		S_2/S_1
		T, °C	μmol H_2/g_{cat}	T, °C	μmol H_2/g_{cat}	
1	Co/Al_2O_3	374	803	660	1651	2.05
2	$Co/(Al_2O_3–10ZSM-5)$	384	799	662	1799	2.25
3	$Co/(Al_2O_3–30ZSM-5)$	380	843	650	1993	2.36
4	$Co/(Al_2O_3–60ZSM-5)$	382	928	622	2361	2.54

These data were used to calculate the degree of dispersion of cobalt (D, %), the degree of reduction of the catalyst (R, %), and the number of active metal sites ($n(Co)^0$) (Table 7) [35, 36]:

$$D = \frac{96}{d_{av}(Co^0)}\%, \quad (5)$$

where $d_{av}(Co^0)$ is the average size of metallic cobalt crystallite (nm);

$$R = \frac{\nu(O_2)\left(\frac{3}{2}\right)Ar(Co)}{m(Co)} \times 100\%, \quad (6)$$

where $\nu(O_2)$ is the amount of absorbed oxygen (mol/g_{cat}), Ar(Co) is the atomic mass of cobalt (g/mol), and m(Co) is the mass of cobalt in the catalyst (g):

$$n(Co^0) = \frac{m(Co)D}{Ar(Co) \times 100}. \quad (7)$$

For all the samples, the cobalt crystallite size is in a range of 3–10 nm. The addition of the zeolite into the composition of the Co/Al_2O_3 catalyst leads to a slight increase in the average crystallite size, namely, from 6 to 7 nm (Table 7).

The degree of reduction of the Co/Al_2O_3 catalyst—24.5%—is the lowest of all the samples (see Table 7). In the case of the zeolite-containing catalysts, the degree of reduction (R) increases from 28.8 to 38.9% owing to a decrease in the amount of cobalt aluminate and the weakening of the interaction of the surface cobalt particles with the support. The addition of the zeolite into the Co/Al_2O_3 catalyst affects (decreases) the degree of dispersion of the active component. The Co/Al_2O_3 catalyst has the highest degree of dispersion: $D = 16.0\%$.

Thus, an increase in the zeolite content in the $Co/(Al_2O_3–ZSM-5)$ catalyst leads to a decrease in the degree of dispersion of the active component; as a consequence, the number of active metal sites $n(Co)^0$ involved in the synthesis reactions decreases from 475 to 425–433 μmol/g_{cat}.

The acidity of the ZSM-5 zeolite and the catalyst samples was measured by NH_3 TPD (Table 8). The highest acidity was observed for the ZSM-5 zeolite (685 μmol NH_3/g_{cat}); the lowest acidity was exhibited by the catalyst sample containing no zeolite (207 μmol NH_3/g_{cat}). The addition of the zeolite into the

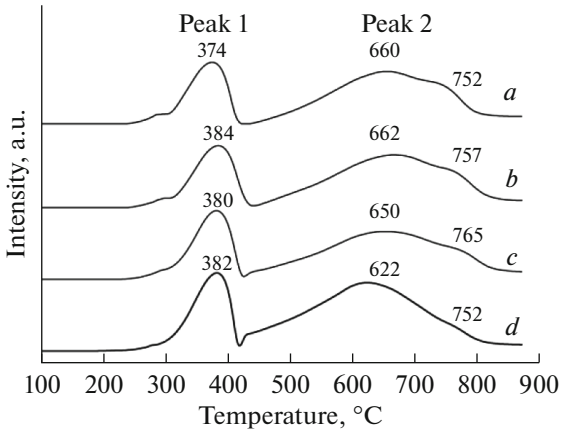

Fig. 4. TPR spectra of the catalyst samples: (*a*) Co/Al_2O_3, (*b*) $Co/(Al_2O_3–10ZSM-5)$, (*c*) $Co/(Al_2O_3–30ZSM-5)$, and (*d*) $Co/(Al_2O_3–60ZSM-5)$.

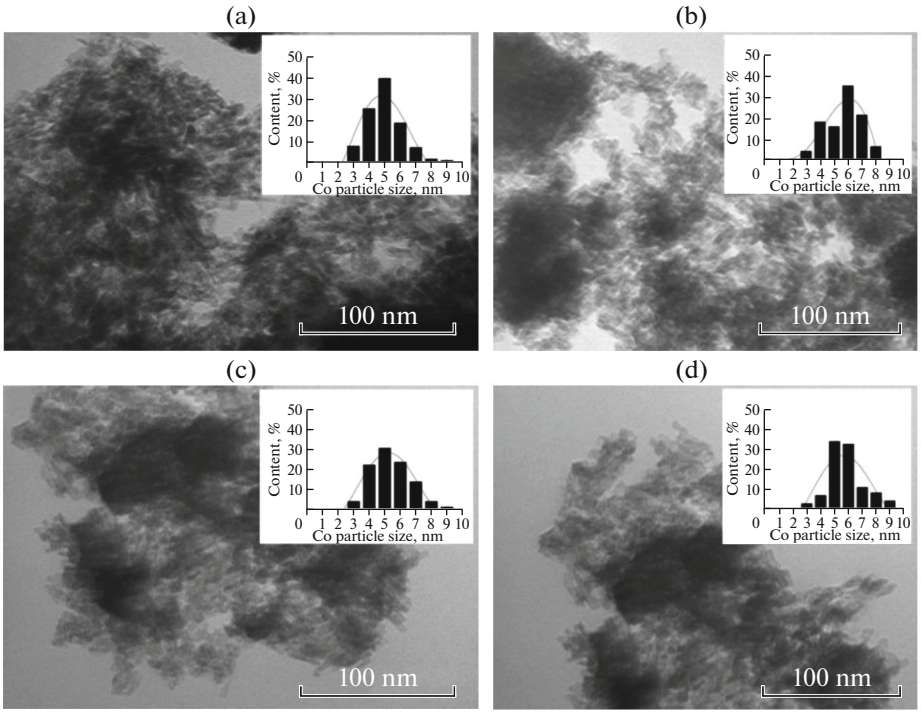

Fig. 5. TEM micrographs of the reduced catalysts and histograms of the cobalt particle size distribution: (a) Co/Al_2O_3, (b) $Co/(Al_2O_3–10ZSM-5)$, (c) $Co/(Al_2O_3–30ZSM-5)$, and (d) $Co/(Al_2O_3–60ZSM-5)$.

Co/Al_2O_3 catalyst leads to an increase in the acid properties of the sample.

An increase in the catalyst acidity affects the process selectivity, as evidenced by an increase in the olefin yield owing to normal C_{5+} paraffins (Fig. 6). The largest—almost threefold—decrease is the content of long-chain C_{19+} HCs in the synthesis products is observed in the presence of the catalyst exhibiting the highest surface acidity.

Thus, the introduction of the ZSM-5 zeolite into the support of the Co/Al_2O_3 HC synthesis catalyst makes it possible to vary the process selectivity for fuel fraction HCs toward an increase in their yield. However, the efficiency of these bifunctional catalysts is lower than that of the Co/Al_2O_3 FT synthesis catalyst (see Table 2). A decrease in the efficiency of the tested catalysts with respect to C_{5+} HCs is symbatic to an increase in the zeolite concentration in the catalyst. This finding can be attributed to both a decrease in the number of active Co^0 metal sites (Table 7) and an increase in diffusion limitations imposed by the introduction of the fine-pored ZSM-5 zeolite into the catalyst composition [38]. It is known [39] that the performance of bifunctional cobalt–zeolite catalyst systems in FT synthesis significantly depends on the acidity and pore structure of the zeolite and the distribution of cobalt in different oxidation states between the pores and the outer surface of the pellets. Another equally important parameter is the degree of dispersion of cobalt crystallites: the degree of dispersion of cobalt is higher in samples with a lower acidity and broad pore channels [38].

In the development of a mechanically strong and highly efficient supported bifunctional catalyst based on a zeolite and a boehmite binder, it is necessary to provide, in addition to mechanical strength, not only an optimum ratio of HC synthesis and hydrotreating sites, but also their accessibility. It can be assumed that

Table 7. Physicochemical properties of the catalysts

Samples	$d_{av}(Co)$, nm	*D*, %	*R*, %	$n(Co)^0$, μmol/g_{cat}
Co/Al_2O_3	6.0 ± 1.1	16.0	24.5	475
$Co/(Al_2O_3–10ZSM-5)$	6.5 ± 1.1	14.7	28.8	446
$Co/(Al_2O_3–30ZSM-5)$	6.6 ± 1.4	14.5	32.8	425
$Co/(Al_2O_3–60ZSM-5)$	7.1 ± 1.4	13.5	38.9	433

Table 8. Total acidity of the zeolite and the supported bifunctional catalyst samples

Sample	Total acidity, μmol NH_3/g_{cat}
ZSM-5	685
Co/Al_2O_3	207
$Co/(Al_2O_3–10ZSM-5)$	287
$Co/(Al_2O_3–30ZSM-5)$	432
$Co/(Al_2O_3–60ZSM-5)$	504

the catalyst should have a developed system of large transport pores, which facilitate the mass transfer of the FT synthesis and cracking products. The search for synthesis methods for these bifunctional catalyst systems by varying the composition and catalyst synthesis techniques is of scientific and practical interest.

CONCLUSIONS

(1) Mechanically strong bifunctional cobalt catalysts for the synthesis of fuel fraction HCs have been synthesized using the ZSM-5 zeolite and a boehmite binder.

(2) It has been found that the efficiency of the supported bifunctional $Co/(Al_2O_3–ZSM-5)$ catalysts is determined by the number of active metal cobalt sites, the degree of dispersion of cobalt crystallites, and the total surface acidity. With an increase in the catalyst acidity, the fuel fraction selectivity increases owing to long-chain HCs. At the same time, the activity of catalysts decreases; therefore, a decrease in their efficiency is observed.

(3) The bifunctional catalyst composition and synthesis method should provide an optimum pore structure to decrease diffusion limitations between the HC synthesis and hydrotreating sites.

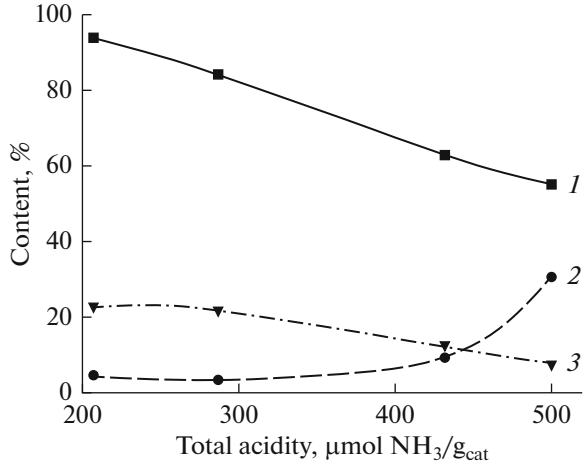

Fig. 6. Dependence of the product composition on the total acidity of the catalysts: (*1*) C_{5+} *n*-paraffins, (*2*) olefins, and (*3*) C_{19+} HCs.

ACKNOWLEDGMENTS

The authors thank OOO Ishimbay Specialized Chemical Catalyst Plant for submitting HZSM-5 zeolite samples and Sasol Germany GmbH (in the person of A. Malyshev) for boehmite samples. This work was supported by the Ministry of Education and Science of the Russian Federation (state task no. 10.2980. 2017/4.6). The work was performed using the equipment of the Center for collective use "Nanotechnology" at the Platov South-Russian State Polytechnic University.

REFERENCES

1. *World Energy Outlook 2011,* Special Report, IEA.
2. C. Kibby and K. Jothimurugesan, T. Das, et al., Catal. Today **215**, 131 (2013).
3. S. S. Ail and S. Dasappa, Renew. Sustain. Energy Rev. **58**, 267 (2016).
4. Y. Wang, W. Zhao, Z. Li, et al., J. Porous Media **22**, 339 (2015).
5. J. T. Bartis, F. Camm, and D. S. Ortiz, *Producing Liquid Fuels from Coal: Prospects and Policy Issues* (RAND Corporation, Santa Monica, CA, 2008), p. 167.
6. A. L. Lapidus and A. Yu. Krylova, Usp. Khim. **67**, 1032 (1998).
7. S. Sartipi, J. E. Dijk, J. Gascon, and F. Kapteijn, Appl. Catal., A **456**, 11 (2013).
8. A. Freitez, K. Pabst, B. Kraushaar-Czarnetzki, and G. Schaub, Ind. Eng. Chem. Res. **50**, 13732 (2011).
9. G. Yang, C. Xing, W. Hirohama, et al., Catal. Today **215**, 29 (2013).
10. Y. Jin, R. Yang, Y. Mori, et al., Appl. Catal., A **456**, 75 (2013).
11. S.-H. Kang, J.-H. Ryu, J.-H. Kim, et al., Catal. Lett. **141**, 1464 (2011).
12. A. P. Savost'yanov, R. E. Yakovenko, G. B. Narochnyi, et al., Izv. Vyssh. Uchebn. Zaved. Severo-Kavkaz. Region., Ser.: Tekh. Nauki, No. **3**, 92 (2016).
13. Q. Zhang, K. Cheng, J. Kang, et al., ChemSusChem **7**, 1251 (2014).
14. G. Espinosa, J. M. Domingueza, P. Morales-Pachecob, et al., Catal. Today **166**, 47 (2011).
15. J. Majewska and B. Michalkiewicz, Int. J. Hydrogen Energy **41**, 8668 (2016).
16. D.-K. Lee, D.-S. Kim, T.-H. Kim, et al. Catal. Today **154**, 237 (2010).
17. S. Sartipi, M. Makkee, F. Kapteijn, and J. Gascon, Catal. Sci. Technol. **4**, 893 (2014).
18. L. V. Sineva, E. Yu. Asalieva, and V. Z. Mordkovich, Usp. Khim. **84**, 1176 (2015).
19. A. Feller, A. Guzman, I. Zuazo, and J. A. Lercher, J. Catal. **224**, 80 (2004).
20. P. V. Lipin, V. P. Doronin, and T. I. Gulyaeva, Pet. Chem. **50**, 362 (2010).

21. L. M. Velichkina, L. N. Vosmerikova, L. L. Korobitsyna, et al., Neftepererab. Neftekhim., No. 1, 13 (2016).
22. S. Sartipi, K. Parashar, M. Makkee, et al., Catal. Sci. Technol. **3**, 572 (2013).
23. S. Sartipi, M. Alberts, M. J. Meijerink, et al., ChemSusChem **6**, 1646 (2013).
24. V. Subramanian, V. L. Zholobenko, K. Cheng, et al., ChemCatChem **8**, 380 (2016).
25. G. Calleja, A. Lucas, and R. Grieken, Fuel **74**, 445 (1995).
26. K. Cheng, L. Zhang, J. Kang, et al., Chem. Eur. J. **20**, 1 (2014).
27. M. Dalil, M. Sohrabi, and S. J. Royaee, J. Ind. Eng. Chem. **18**, 690 (2012).
28. *PDF-2: The Powder Diffraction File*^{TM} (ICDD, 2014). www.icdd.com.
29. R. A. Young, *The Rietveld Method* (Oxford University Press, Oxford, 1995).
30. A. P. Savost'yanov, R. E. Yakovenko, G. B. Narochnyi, et al., Kinet. Catal. **58**, 81 (2017).
31. F. Pardo-Tarifa, S. Cabrera, M. Sanchez-Dominguez, and M. Boutonnet, Int. J. Hydrogen Energy **42**, 9754 (2017).
32. G. Jacobs, T. K. Das, Y. Zhang, et al., Appl. Catal., A **233**, 263 (2002).
33. M. J. Parnian, A. T. Najafabadi, Y. Mortazavi, et al., Appl. Surf. Sci. **313**, 183 (2014).
34. Z. Hou, J. Gao, J. Guo, et al., J. Catal. **250**, 331 (2007).
35. S. Wang, Q. Yin, J. Guo, et al., Fuel **108**, 597 (2013).
36. A. Tavasoli, R. M. Abbasloua, M. Trepanier, and A. K. Dalai, Appl. Catal., A **345**, 134 (2008).
37. F. Lonyi and J. Valyon, Microporous Mesoporous Mater. **47**, 293 (2001).
38. S. Bessell, Appl. Catal., A **126**, 235 (1995).
39. V. Subramanian, V. L. Zholobenko, K. Cheng, et al., ChemCatChem **8**, 380 (2016).

Translated by M. Timoshinina